The interaction of cnoidal waves with oscillating wave surge energy converters

Daniela Benites Munoz, Luofeng Huang, Giles Thomas
University College London, United Kingdom

Among wave energy conversion devices, the Oscillating Wave Surge Converter (OWSC) stands out as an efficient and stable solution. These devices are composed of a buoyant flap that rotates around a hinge fixed close to the seabed. An ongoing challenge is to predict the hydrodynamic loads on the devices, as the device will at times operate under rough sea states, when wave slamming can cause high peak pressures. The aim of this study is to predict the peak pressure loads obtained during wave slamming using numerical simulations. To achieve this, a two-dimensional model of an OWSC within a Numerical Wave Tank (NWT) was developed in OpenFOAM. The model setup was based on an existent experimental test in which the OWSC was placed as a rigid body-fitted flap, while the experimental wave was made using the cnoidal wave theory. The discretisation of the mesh surrounding the body was handled by using overset-mesh technology, allowing the high-amplitude rotations of the OWSC. Based on the built model, the interaction of waves with OWSC has shown to be reasonably simulated, and the process is analysed in detail. After validation against experiments, the model also shows good accuracies on predicting the peak pressure loads and the rotation of the flap, while it underestimates the negative peak velocities.

1 Introduction

Among oscillating body converters, there is a subgroup of devices harnessing the horizontal acceleration of the waves' particles referred to as Oscillating Wave Surge Converters (OWSC). These converters are composed of a surface-piercing buoyant flap that rotates around a hinge fixed close to the seabed. Due to the rough sea conditions where OWSC usually operate, sudden short peak pressure loads acting near the centre of the flap have been identified [18][20]. This phenomenon, known as wave slamming, occurs when the relative velocity between the flap and the incident wave is high. The prediction of extreme pressure during wave slamming has become a key challenge in OSWC design [4][20].

In 2012, a test campaign using a 25th model was done in Queen's University Belfast (QUB); among the reported results, short peaks of pressure acting on the seaward surface of the flap were observed [5]. These high impulsive loads presented at the maximum rotational velocities of the flap were related to slamming. An extension of this work was developed developed through a two-dimensional experimental test in the Ecole Centrale Marseille (ECM) using a 1:40 scale model [4][3]. The aim of these tests was to investigate the response of the flap-type device to these short-period high-peak wave loads occurring under extreme sea conditions. Moreover, to understand the fundamentals and key parameters of wave slamming, specifically, the distribution of the pressure on the flap's face presented during this event. Both experiments were two-dimensional, i.e. the width of the flap was almost the same as the width of the wave flume. In addition, air pockets were spotted near the contact point (free surface level) along with the presence of the high-peak loads [4][3]. Pressure oscillations were identified near the contact point of the incident wave during the experimental testing; these were thought to be related to the air bubbles visualised in the same area [3].

Considering the flap-type geometry of the OSWC, this type of device can be analysed with linear wave theory when operating under normal sea conditions (low wave steepness). However, to include complex phenomena, such as slamming, nonlinear numerical approaches are more suitable, such as solving Reynolds averaged Navier-Stokes

(RANS) equations using Computational Fluid Dynamics (CFD).

Some studies of the hydrodynamic response of OWSC to ocean waves have been carried out using the open-source software OpenFOAM. They have been found to deal with the wave-structure interaction phenomenon effectively [5][16][20][21][13]. The numerical results obtained in [20] using a commercial software are in fairly good agreement with the test results obtained in the wave flume of ECM and they have captured the peak rotation and angular velocities values during the wave slamming event. However, the numerical and experimental data/results are thought to be affected by reflected waves and the air pockets were not captured in the numerical simulation. In other numerical studies, such as the one undertaken by [13], the initial reported results under predict the angle of rotation and angular velocity of the OWSC against the experimental results. This was attributed to the poor matching of wave; however, the numerical results were finally improved by refining the mesh. The high loads due to wave slamming occur in the centre of the flap and therefore, the use of two-dimensional (2D) numerical models is expected to roughly estimate these loads without the use of a three-dimensional (3D) one [20]. This is because the peak-loads distribution produced by wave slamming decrease in direction to the sides of the flap. By using 2D models against 3D models, the computational effort reduces significantly.

One gap in previous work is that the body-fit dynamic mesh is only capable of simulating small body displacements. As large-range rotations are expected to occur with OWSC, this work incorporates the overset mesh technique to handle the large structural movement. Section 2 introduces a set of OpenFOAM theories and practicalities for simulating the OSWC problem, including the implementation of overset mesh around the structure. Section 3 presents the validation of the model and further investigates the wave-structure interaction in detail; particularly, the timing of wave slamming in the periodical process has been identified. In the final section, the implications and limitations of current work are discussed.

2 Numerical Approach

For the numerical model of the flap-type OWSC, a Numerical Wave Tank (NWT) is developed using the open-source software OpenFOAM. two immiscible fluids, water and air, and, the moving surface connecting them (free surface) are considered for the NWT. These fluids are assumed to be incompressible. The governing equations for this multiphase system include the continuity and momentum equations, the latter of which deals with the force balance due to the pressure, gravity, and viscous effects. The equations presented below govern the motion of incompressible Newtonian fluids [6][10]:

$$\nabla \cdot \boldsymbol{U} = 0 \qquad (1)$$

$$\frac{\partial \rho \boldsymbol{U}}{\partial t} + \nabla \cdot [\rho \boldsymbol{U} \boldsymbol{U}^T] = -\nabla p^* - \boldsymbol{g} \cdot \boldsymbol{x} \nabla \rho$$
$$+ \nabla \cdot [\mu \nabla \boldsymbol{U} + \rho \boldsymbol{\tau_R}] + \sigma \kappa \nabla \alpha \qquad (2)$$

In these equations, $\boldsymbol{U}$ and $\boldsymbol{g}$ are used for the velocity and gravity vector fields, respectively. The variable ρ is the density, p^* is the pseudo-dynamic pressure $p = \rho \boldsymbol{g} \cdot \boldsymbol{x}$ (used as a numerical technique for the solution), $\boldsymbol{x}$ is the position vector and μ is the dynamic viscosity. The Reynolds stress tensor is represented by $\boldsymbol{\tau_R}$. The last term is the effect of surface tension, which can be neglected for large scale flows [19]. In OpenFOAM, the solution of the governing equations to estimate the pressure and velocity across the multiphase system is achieved using the Finite Volume Method (FVM) of discretisation. Additionally, the Volume of Fluid (VoF) approach was used to capture the interface between the air and the water.

In the VoF method [7], a volume fraction constant, α, is introduced to identify the quantity of liquid in each cell of the model. If α is equal to 1 the cell is filled with water, whereas if it is 0, the cell is filled with air. In the case where α has a value between 0 and 1, that cell has part water and part air, and therefore, these cells contain the free surface. Field values such as the velocity $\boldsymbol{U}$, the density ρ and the dynamic viscosity μ of the cell are calculated using the weighted average field value of each fluid. The variation of the volume fraction is done using the advection equation. This is the Equation 3 which tracks the fluid interface movement and is solved simultaneously with Equations 1 and 2 to solve the multiphase system:

$$\frac{\partial \alpha}{\partial t} + \nabla \cdot (\boldsymbol{U} \alpha) = 0 \qquad (3)$$

For the velocity-pressure coupling solution, the PIMPLE algorithm is used, this is a mixture of the PISO (Pressure Implicit with Splitting of Operators) and SIMPLE (Semi-Implicit Method for Pressure-Linked Equations) solving procedures. The main structure of PIMPLE is based on the PISO solver, but the stability of the solution is improved; less iterations are required for the solution and the simulation speed is incremented [2][11].

To close the equations for the solution of the RANS equations, the k-ω (Shear Stress Tensor,

SST) turbulence model is used, which has been successfully used for wave-structure interaction for high pressure gradients and flow separation [16].

The dimensions of the numerical tank are 16.77 x 0.70 meters (length x height), based on the experimental setup presented in [4][3]. The physical boundary conditions, or patches, of the 2D model include the inlet, outlet, atmosphere, bottom, front and back boundary conditions, are presented in Figure 1. At the inlet and outlet the velocity field boundary condition is prescribed considering the theoretical velocity value according to the wave theory applied [6]; whilst in both faces, the pressure is considered to be adapted to this theoretical velocity value. The bottom considers the geometrical constraint of wall and the no-slip condition is applied. For the atmosphere, the open boundary condition is considered.
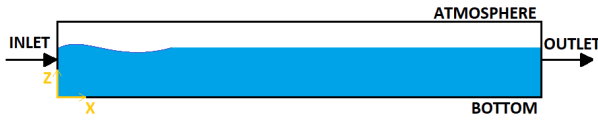

Figure 1: Schematic of the Numerical Wave Tank with applied boundary conditions.

The computational domain is discretised into non-overlapping finite volumes, or cells, in which the algebraic equations are solved to obtain the pressure, volume of fraction, and velocity fields of the fluid system. Due to the simple rectangular geometry of the NWT, *blockMesh* application is used to generate the mesh.

The OWSC model is simplified as a rigid body-fitted plate located within the tank. The discretisation of the mesh surrounding the body is handled by an overlapping mesh (overset or Chimera mesh) and is independent of the one used for the NWT. The width of the overlapping zone is defined according to the geometry of the structure of analysis and the expected motion. Following, the cells and points conforming the OWSC are removed from the domain of the overlapped mesh, this is called *hole cutting*. After the *hole cutting* is done at the beginning of the simulation, the communication of the two meshes is done at every time-step through the *domain connectivity information* (DCI). In this region, the fringe cells (located at the outer boundary of the overset mesh) are the interpolation cells connected to donor stencils from the background mesh. The other cells, or CV, inside the overset mesh are discretisation cells of the previously mentioned mesh [12].

To build the OWSC device, a box shape of the same dimensions of the 1:40 scale test model was used, these being 0.88 m x 0.04 m x 0.31 m (thickness x width x height). The model is located

at 12.20 m from the wave-maker and the hinge height from the flume bottom to the hinge this distance is 0.12 m.

After the convergence study of the mesh using a refinement ratio of $\sqrt{2}$ [17][9] the square cell size for this model is 0.01 m for the NWT domain, with 550 cells per wavelength and 12 cells per wave height, whereas for the region of the overset mesh the cell size is 0.0025 m. Nonetheless, the mesh is refined in the region surrounding the body and the free surface, see Figure 2. In this case, the size of the background mesh cells near the OWSC is 0.005 m x 0.005 m. As it is a two-dimensional model, in the y-direction a unit cell is considered.
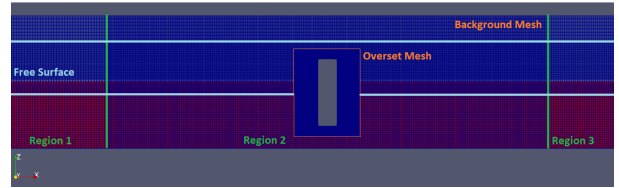

Figure 2: Background and overset mesh. The regions of interest (Region 2 and Free Surface) are refined in order to capture the wave profile and OWSC body motion.

The temporal discretisation used is adjusted during the simulation according to a strict limit on the Courant Number, *CFL*. This number relates to the quantity of a specific value, in this case, the velocity flux U_x, crossing a grid cell Δx in a given time-step Δt. As a result, the *Co* is a reference of the stability of the simulation and is defined as:

$$CFL = \frac{U_x \Delta t}{\Delta x} \tag{4}$$

For multiphase simulations the *CFL* is recommended to have a maximum value of 0.25 [8], and by using adjustable time discretisation, the time-step used will be fixed according to the estimated value of the velocity in the cell, the size of the cell and the limit of *CFL*.

According to the cnoidal wave theory, continuous waves are generated using fixed value (Dirichlet type) boundary conditions at the inlet of the NWT, as presented in [6]. The pressure is calculated within the numerical model whilst the values of the velocity fields and the free surface elevation are corrected in the wave generation patch according to the wave theory applied. The free surface is measured at the patch at each time step and compared to the theoretical value, and, corrected accordingly by modifying the U and α boundary conditions. The static boundary wave generator is combined with active wave absorption, and by thus, dissipation zones are not needed, and unnecessary water level increase is avoided. The

methodology is further detailed in [6]. The wave height considered is H = 0.1 m, and the period, T = 1.9 s. The depth in this condition was 0.305 m. The fluid forces, $\boldsymbol{F}$, considered are the surface forces (pressure, normal and shear stresses), $\boldsymbol{F_s}$, as well as the body forces (gravitational forces), $\boldsymbol{F_b}$. The surface forces are calculated at each time-step of the numerical simulation by integrating the pressure and the viscous stress components over the wetted surface of the rigid body, S_B, whilst the body forces include the gravitational force, as follows:

$$\boldsymbol{F} = \boldsymbol{F_s} + \boldsymbol{F_b} = \int_S (-p\boldsymbol{I} + \boldsymbol{\tau}) \cdot \boldsymbol{n} dS + m\boldsymbol{g} \quad (5)$$

Where p is the pressure, $\boldsymbol{I}$ is the unit or identity tensor of size (3x3), $\boldsymbol{\tau}$ is the viscous stress tensor, $\boldsymbol{n}$ is the unit normal vector to the body surface, m is the mass of the rigid body, $\boldsymbol{g}$ is the acceleration of the gravity vector and S_B is the wetted surface. Similarly, the total moment, $\boldsymbol{M}$, is calculated at each time-step as the sum of all the components acting around the hinge of the OWSC device:

$$\boldsymbol{M} = \int_S \boldsymbol{r} \times (-p\boldsymbol{I} + \boldsymbol{\tau}) \cdot \boldsymbol{n} dS + (\boldsymbol{CoG} - \boldsymbol{x_H}) \times m\boldsymbol{g}$$
$$(6)$$

where $\boldsymbol{r}$ is the is the position vector (x, y, z), $\boldsymbol{CoG}$ is the position of the centre of gravity at a time-step and The motion equation for the rigid body is based on the linear and angular momentum equations:

$$\boldsymbol{a} = \frac{\boldsymbol{F}}{m} \quad (7)$$

$$\boldsymbol{\theta} = \frac{\boldsymbol{M}}{I_m} \quad (8)$$

where $\boldsymbol{a}$ and $\boldsymbol{\theta}$, are the linear and angular acceleration, respectively, and I_m is the moment of inertia of the rigid body.
For the numerical simulation, the Newmark time integration scheme is applied to obtain the velocity and displacement of the rigid body [14]. The linear velocities and the displacements of the body are obtained from the following equations [15]:

$$\boldsymbol{U}_b^{t+\Delta t} = \boldsymbol{U}_b^t + [(1-\gamma)\boldsymbol{a}^t + \gamma\boldsymbol{a}^{t+\Delta t}]\Delta t \quad (9)$$

$$\boldsymbol{x}_b^{t+\Delta t} = \boldsymbol{x}_b^t + \boldsymbol{U}_b^t\Delta t + [(\frac{1}{2} - \beta)\boldsymbol{a}^t + \beta\boldsymbol{a}^{t+\Delta t}]\Delta t^2 \quad (10)$$

where $\boldsymbol{U}_b$ is the velocity vector of the body, $\boldsymbol{x}_b$ is the displacement vector of the body, γ is the velocity integration coefficient, β is the position integration coefficient, Δt is the time-step, super script t is used for the values obtained on the previous iteration, whilst $t + \Delta t$ is for the values at the current time being simulated. The recommended values for γ is 0.5, whilst for β is 0.25 [1], which are the ones used in this simulation. The motion of the body is handled by the *sixDoFRigidBodyMotion* solver.

3 Results and discussion

3.1 Validation

To check the quality of wave generation and propagation, the wave elevation is measured at 5.2 m from the inlet and compared with the corresponding experimental data of [4]. The approximated wave is fairly slightly under predicted when compared to the experimental wave in the through. However, as it can be seen in Figure 3, in both cases, the numerical and experimental tests, it is difficult to maintain the monochromatic wave without being affected by the reflection of the waves caused by the motion of the OWSC. This can be seen as slight deviations between both curves. Nonetheless, due to certain imperfection of experimental waves, it is considered that the numerical wave is reasonably modelled.
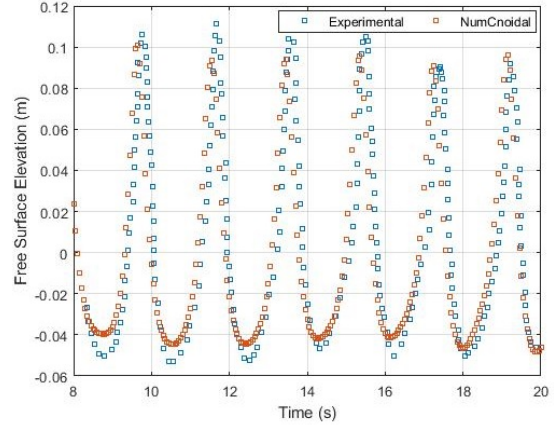

Figure 3: Free surface elevation at 5.2m from the wave maker patch, measured numerically and experimentally.

Within the results obtained, and compared to the experimental ones [4], are the rotation angle and the angular velocity of the OWSC model, in Figure 4 and Figure 5, respectively. In the trough the maximum relative error is 11%, whereas, in the crests, this difference is close to 6%. These errors are similarly reproduced in the case of the angular velocities shown in Figure 5, but in this case, the relative error is significantly higher, being 40% in the trough, specifically in capturing the short-period peak velocity. The negative angular velocity is when the flap is pitching seaward (in the direction to the wave maker). The reason of the error obtained needs further investigation, since mesh sensitivity tests for

the body accelerations have been done thoroughly. Despite the peak pressure is not captured numerically, in experiment it also appears in a very short time, thus the corresponding impulse is not pronounced so the movement of OWSC are still accordant in both methods.
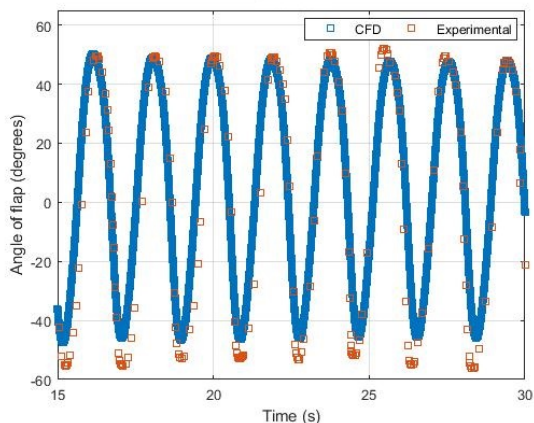

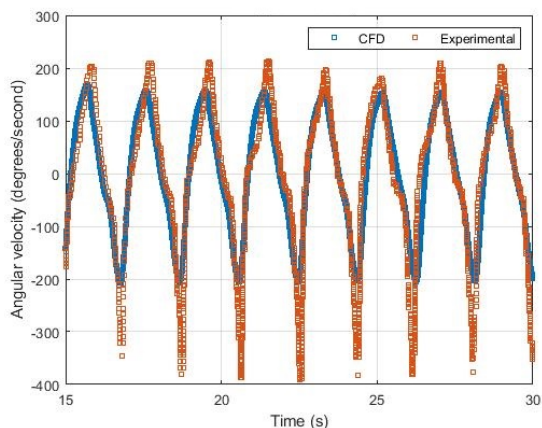Figure 4: Experimental and numerical results of the flap's rotation angle.

Figure 5: Experimental and numerical results of the flap's angular velocity.

3.2 Wave-structure interaction

As said previously, the slam loading event can be identified by a large increase in the pressure within a short period of time and is influenced by the angle of contact and relative rotational motion between the flap-type device and the incident wave. In the experimental test, the pressure reaches the peak in 0.03 s whilst in the numerical test, takes 10 times longer (0.30 s); nonetheless, the magnitude achieved by the numerical model is similar to that obtained experimentally (12 kPa, measured at the point of contact of the flap and the free surface). In Figure 6, the maximum pressure of 12.21 kPa is
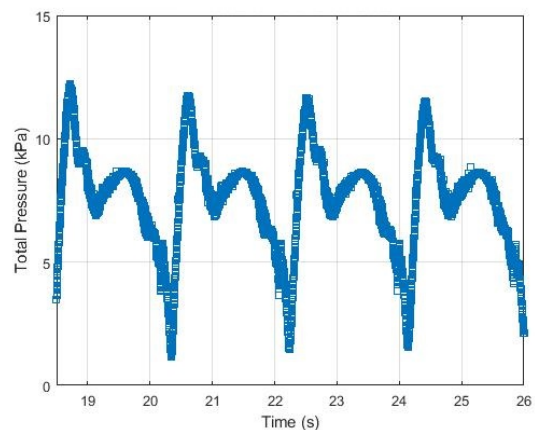
seen at 18.7s.

Figure 6: Total pressure measured at water line level in the seaward side of the flap (0.305 m).

One period sequence of the simulation is shown in Figure 7, along with the results of the angle of rotation, angular velocities and pressure. In Frame (A), the maximum rotation of the device is facing opposite to the wave generation patch, the angular velocity is zero and the pressure measured in the contact surface of the flap at still water level is large. When the water runs down the flap, the pressure drops to zero in the absence of water in this region (see Frames (B) and (C)), whereas the negative angular velocity increases, and the flap returns to its initial position in Frame (C), where the rotation is 0. In Frame (D) the wave runs up the flap, the negative angular velocity reaches the minimum value, and the rotation of the flap changes the direction, to reach the largest angle in the seaward direction (Frame I), where the angular velocity is zero. The pressure loads acting on the flaps surface increases suddenly from Frames (E) to (F).

4 Conclusions

A 2D-numerical model has been developed to simulate the movement of an OWSC device in cnoidal waves. The numerical approach used has been introduced in detail and subsequently simulations presented to show that the behaviour of the device is modelled reasonably successfully. After validation against experiments, the numerical results are shown to be generally accurate but a large deviation appears in the prediction of the angular velocity of the device, which will need to be examined further. Further work could consider examining the hydrodynamic response of OWSC under more advanced sea conditions, e.g. irregular waves.
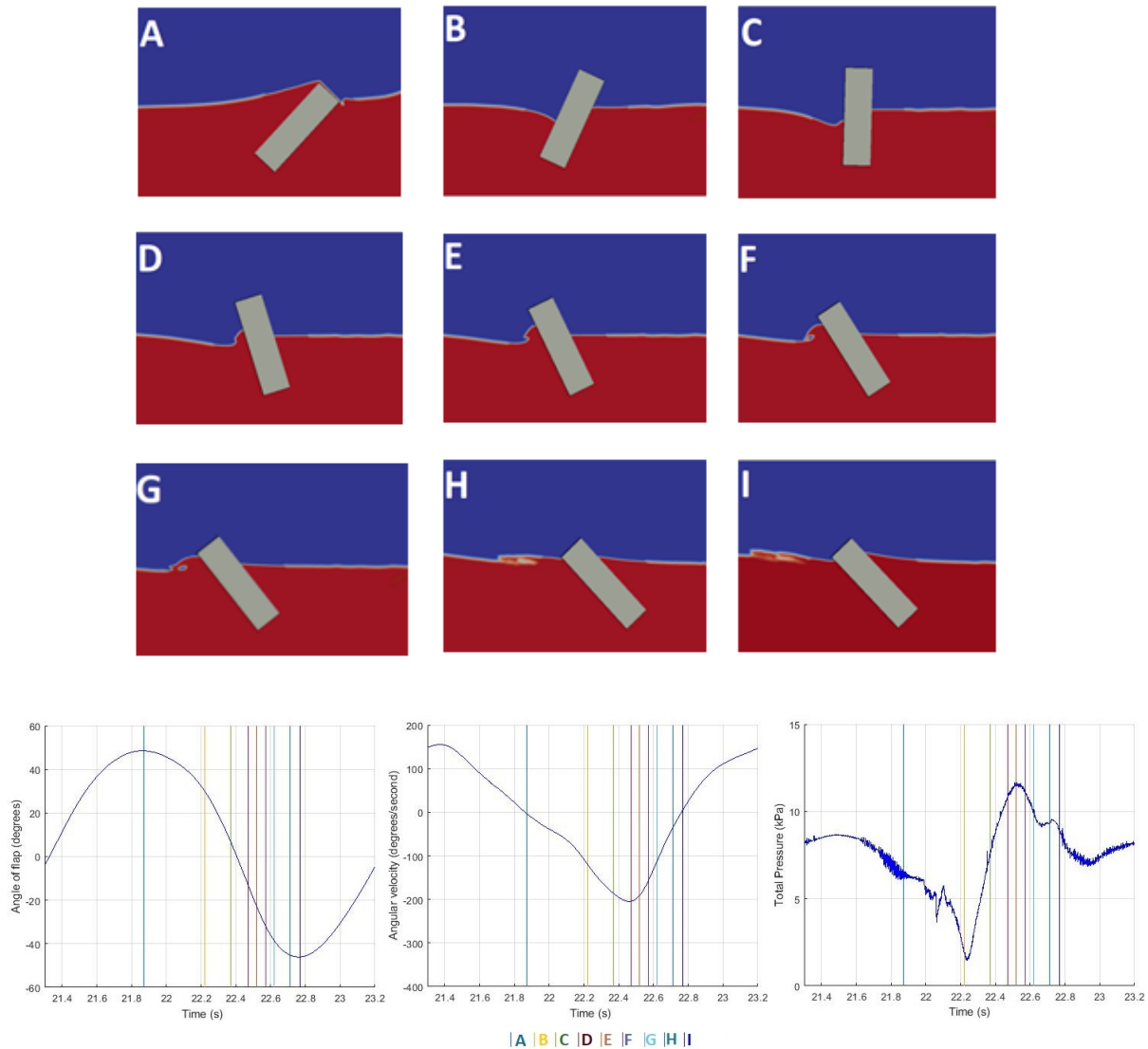
Figure 7: Time series presenting one period of the OWSC movement and the corresponding angle of rotation, angular velocity and pressure measured at the initial point of contact of the flap with the still water level (this is at 0.205 m height measured in the plate).

References

[1] H.A. Moossavi Buchholdt and S.E. Nejad. Response of linear and non-linear one degree-of-freedom systems to random loading : time domain analysis. In *Structural Dynamics for Engineers (2nd Edition)*, chapter 6, pages 117–135. 2012.

[2] Joel H Ferziger and Milovan Peric. *Computational Methods for Fluid Dynamics*. 2002.

[3] Alan Henry, Thomas Abadie, Jonathan Nicholson, Alan Mckinley, Olivier Kimmoun, and Frederic Dias. The Vertical Distribution and Evolution of Slam Pressure on an Oscillating Wave Surge Converter. pages 1–11, 2015.

[4] Alan Henry, Olivier Kimmoun, Jonathan Nicholson, Guillaume Dupont, Yanji Wei, and Frederic Dias. A two dimensional experimental investigation of slamming of an Oscillating Wave Surge Converter. *Proceedings of the International Offshore and Polar Engineering Conference*, (January):296–305, 2014.

[5] Alan Henry, Ashkan Rafiee, Pal Schmitt, Frederic Dias, and Trevor Whittaker. The Characteristics of Wave Impacts on an Oscillating Wave Surge Converter. *Journal of Ocean and Wind Energy*, 1(2):101–110, 2013.

[6] Pablo Higuera, Javier L. Lara, and Inigo J. Losada. Simulating coastal engineering processes with OpenFOAM®. *Coastal Engineering*, 71:119–134, jan 2013.

[7] C.W Hirt and B.D Nichols. Volume of fluid (VOF) method for the dynamics of free boundaries. *Journal of Computational Physics*, 39(1):201–225, jan 1981.

[8] Zheng Zheng Hu, Deborah Greaves, and Alison Raby. Numerical wave tank study of extreme waves and wave-structure interaction using OpenFoam®. *Ocean Engineering*, 126(March 2015):329–342, 2016.

[9] ITTC. Uncertainty Analysis in CFD Verification and Validation, Methodology and Procedures. In *International Towing Tank Conference*, 2017.

[10] Niels G. Jacobsen, David R. Fuhrman, and Jørgen Fredsøe. A wave generation toolbox for the open-source CFD library: OpenFoam®. *International Journal for Numerical Methods in Fluids*, 70(9):1073–1088, 2012.

[11] H Jasak. Error Analysis and Estimation for the Finite Volume Method with Applications to Fluid Flows. *Direct*, M(June):394, 1996.

[12] Z.H. Ma, L. Qian, P.J. Martínez-Ferrer, D.M. Causon, C.G. Mingham, and W. Bai. An overset mesh based multiphase flow solver for water entry problems. *Computers & Fluids*, 172:689–705, aug 2018.

[13] Pedro J. Martínez-Ferrer, Ling Qian, Zhihua Ma, Derek M. Causon, and Clive G. Mingham. Improved numerical wave generation for modelling ocean and coastal engineering problems. *Ocean Engineering*, 152(September 2017):257–272, 2018.

[14] N. M. Newmark. A method of computation for structural dynamics. *Journal of the Engineering Mechanics Division*, 1959.

[15] P. Frank. Pai. *Highly Flexible Structures - Modeling, Computation, and Experimentation*. American Institute of Aeronautics and Astronautics, 2007.

[16] Pal Schmitt and Bjorn Elsaesser. On the use of OpenFOAM to model oscillating wave surge converters. *Ocean Engineering*, 108:98–104, 2015.

[17] Fred Stern, Robert V Wilson, Hugh W Coleman, and Eric G Paterson. Comprehensive Approach to Verification and Validation of CFD Simulations, Part 1 : Methodology and Procedures. *Journal of Fluids Engineering*, 123(December 2001):793–802, 2001.

[18] S. Y. Sun, S. L. Sun, and G. X. Wu. Oblique water entry of a wedge into waves with gravity effect. 52:49–64, 2015.

[19] Vuko Vukčević. Numerical Modelling of Coupled Potential and Viscous Flow for Marine Applications. Technical report, 2016.

[20] Yanji Wei, Thomas Abadie, Alan Henry, and Frédéric Dias. Wave interaction with an Oscillating Wave Surge Converter. Part II: Slamming. *Ocean Engineering*, 2016.

[21] Yanji Wei, Ashkan Rafiee, Alan Henry, and Frédéric Dias. Wave interaction with an Oscillating Wave Surge Converter. Part I: Viscous effects. *Ocean Engineering*, 113:319–334, 2016.